Water Oxidation

DOI: 10.1002/ange.201201356

Ligand Geometry Directs O–O Bond-Formation Pathway in Ruthenium-Based Water Oxidation Catalyst**

*Somnath Maji, Laura Vigara, Francesca Cottone, Fernando Bozoglian, Jordi Benet-Buchholz, and Antoni Llobet**

Four-electron oxidation of water to molecular dioxygen is one of the key steps that needs to be fully solved to be able to develop new sustainable energy conversion schemes based on water splitting by sunlight.[1] In addition, this reaction is also one of the crucial steps that occur in the oxygen evolving center of photosystem II (OEC-PSII) in green plants and algae.[2] Therefore the understanding of how water oxidation occurs at a molecular level is nowadays one of the most important challenges faced by the scientific community, and by extension to our society, which needs an urgent energy solution.[3]

The initial development of the water oxidation catalysis field was based on dinuclear ruthenium complexes[4] bearing polypyridyl-type ligands. Recently this family of catalysts has been extended to mononuclear ruthenium complexes[5] as well as to other first-[6] and third-row[7] transition-metal complexes. Despite these important developments, the mechanistic description of the different pathways under which these reactions take place, together with the full spectroscopic characterization of reaction intermediates, is still a formidable challenge. We and others have contributed significantly towards this endeavor based on kinetics and mainly UV/Vis spectroscopy. In addition ^{18}O-labeling experiments can be a tremendously informative mechanistic tool, given the fact that one of the critical steps in water oxidation is the formation of O–O bonds, as has been put forward in previous mechanistic examples.[8]

Herein we present the synthesis and spectroscopic and electrochemical characterization of new water oxidation catalyst, **2**, which contains the dinucleating bpp^- ligand and the facial tpym ligand (see Figure 1 for a crystal structure and Table 1 for ligand structures and compound numbering). Further we also report a mechanistic description of the water oxidation reaction based on kinetics and supporting by ^{18}O-labeling experiments.

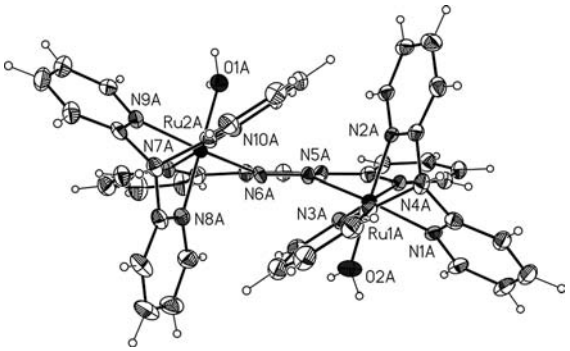

Figure 1. Ortep plot for the X-ray structure of the cationic portion of *P*-**2** with ellipsoids drawn at 50% probability.

Table 1: Drawn ligand structures and complex numbering scheme discussed in this paper.[a]

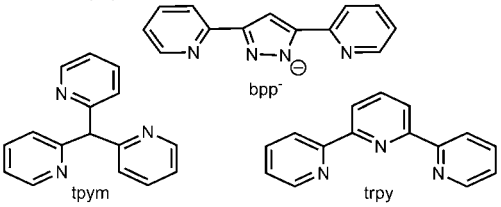

Complex	Structure
1	*trans*-{[Ru^{II}(tpym)(Cl)]$_2$(μ-bpp)}(PF_6)
2	*trans*-{[Ru^{II}(tpym)(H_2O)]$_2$(μ-bpp)}$(PF_6)_3$
3	*trans,fac*-{[Ru^{II}(bpea)(Cl)]$_2$(μ-bpp)}(PF_6)
4	*trans,fac*-{[Ru^{II}(bpea)(H_2O)]$_2$(μ-bpp)}$(PF_6)_3$
5	{[Ru^{II}(trpy)]$_2$(μ-bpp)(μ-Cl)}$(PF_6)_2$
6	*cis*-{[Ru^{II}(trpy)(H_2O)]$_2$(μ-bpp)}$(PF_6)_3$

[a] bpea = bis(2-pyridyl)ethylamine, bpp^- = 3,5-bis(2-pyridyl)pyrazolate, tpym = tris-(2-pyridyl)methane, trpy = 2,2′:6′,2″-terpyridine.

The dinuclear *trans*-Ru-OH_2 complex **2** is prepared in good yield by stoichiometric addition of Ag^+ to a solution of the corresponding Ru-Cl complex **1**. The latter in turn is obtained by reacting 2 equivalents of $RuCl_3$ and tpym with the deprotonated dinucleating tetraaza bridging bpp^- ligand. Figure 1 shows the X-ray structure of the cationic moiety of **2**, wherein the two Ru centers present a distorted octahedral geometry resulting from the constraints imposed by the multidentate ligands.

While bond distances and angles are unremarkable[9] the relative disposition of the Ru centers and particularly their Ru-aqua groups is very interesting. They are arranged with

[*] Dr. S. Maji, Dr. L. Vigara, F. Cottone, Dr. F. Bozoglian, Dr. J. Benet-Buchholz, Prof. A. Llobet
Institute of Chemical Research of Catalonia (ICIQ)
Av. Paisos Catalans 16, 43007 Tarragona (Spain)
E-mail: allobet@iciq.es
Prof. A. Llobet
Departament de Química, Universitat Autònoma de Barcelona
08193 Barcelona (Spain)
and
Department of Bioinspired Science, Ewha Womens University
120-750 Seoul (Korea)

[**] Support from the MICINN (CTQ2010–21497) and the WCU Program (R31-10010) Korea are gratefully acknowledged. S.M. thanks the MICINN for a Torres Quevedo contract.

Supporting information for this article is available on the WWW under http://dx.doi.org/10.1002/anie.201201356.

a RuO-ORu torsion angle of 133.9°, which is 46.1° away from 180° for an ideal octahedral symmetry. This singular arrangement is a consequence of the restricted space available for the two facial tpym ligands which once coordinated, display a π-stacking interaction between two of their pyridyl groups (rings containing the N10A and N3A atoms). Furthermore, there is also an inverse relative rotation of the bpp^- pyridyl groups (rings containing the N4A and N7A atoms) which places the Ru centers above and below the plane of the pyrazolate moiety, and thus is responsible for the generation of the two helical enantiomers that are found in the unit cell of the crystal structure.

We have previously reported the related Ru dinuclear complexes **3** and **4**,[10] wherein the facial tpym ligands are replaced by bpea ligands. In this case the less sterically demanding bpea ligand allows a dihedral angle of the monodentate ligands of 166.3°, which is much closer to the ideal 180°.

Redox properties of **1** and **2** were investigated by means of cyclic voltammetry (CV) and square wave voltammetry (SQWV), and the most significant features are presented in Figure 2 and in Table 1 together with those of complexes **3**–**6**

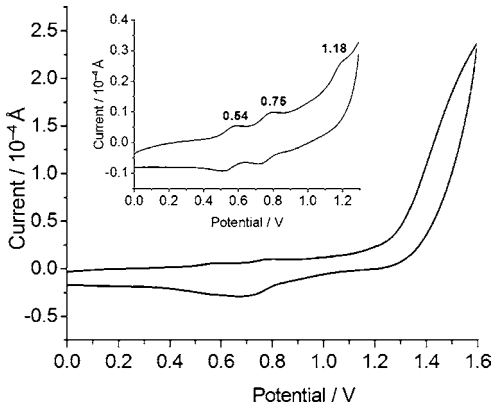

Figure 2. Cyclic voltammetry of **2** at pH 1.0 on a glassy carbon disk working electrode using Pt wire as an auxiliary and SSCE as reference electrodes. Scan rate 100 $mV s^{-1}$. Inset: a new CV experiment under the same conditions but in the 0.0 to 1.25 V range.

for comparison purposes. Complexes **5** and **6** are the related complexes in which the tridentate facial ligands tpym or bpea are replaced by the tridentate meridional trpy ligands. The meridional geometry of the tridentate ligand generates a dramatic change in the relative orientation of the aqua and Cl ligands, thus producing a *cis* geometry. While complex **6** has the same number of coordinating ligands as **2** and **4**, complex **5** possesses a single Cl atom bridging the two metal centers.[11]

As can be observed in Table 2, the redox potentials for the III,III–III,II and III,II–II,II couples, measured in CH_2Cl_2 as the solvent, are shifted anodically by 120 and 170 mV, respectively in **1** with respect to that of **3**. This shift is a consequence of both the lower σ-donating and higher π-accepting capacity of the tpym ligand in **1**, relative to that of bpea in **3**, and thus manifests in the dramatic changes the

Table 2: Redox potentials $E_{1/2}$ [V] at pH 1.0 vs. SSCE for complex **1** and **2** as described in this work and for related dinuclear complexes.

	III,II/II,II	III,III/III,II	IV,III/III,III	IV,IV/IV,III
1	0.54	0.84	–	–
3	0.37	0.72	–	–
5	0.71	1.12	–	–
2	0.54	0.75	1.18	1.52
4	0.21	0.43	0.61	–
6	0.59	0.65	0.88	1.10

tridentate auxiliary ligands exert over the Ru metal center. This effect is a fundamental factor influencing the substitution kinetics of the monodentate ligands in this family of complexes, and thus determines the oxygen-labeling feasibility.[9f] For the case of **5** the potentials are not easily comparable because of the fact that it only contains one Cl ligand bridging the Ru centers. Furthermore, in the case of **5** the two Ru centers interact through both pyrazolato and Cl bridging groups, thus generating a different electronic coupling than in the case of **1** and **3**, which have a single bridging pyrazolato ligand.[12] The anodic shift is also observed for the Ru-OH_2 complexes measured at pH 1.0 in 0.1 M triflic acid, where potentials for the IV,III–III,III, III,III–III,II, and III,II–II,II couples are shifted by 570, 320, and 330 mV, respectively, for **2** relative to **4**. Changing the facial tpym ligand by meridional trpy increases the the III,II–II,II couple but decreases the IV,III–III,III and the III,III–III,II redox potentials by 100 and 300 mV, respectively. For complex **2** one more wave is observed at 1.52 V, which is assigned to the IV,IV–IV,III couple (see SQWV in the Supporting Information) and that is associated with an electrocatalytic current because of the catalytic oxidation of water into dioxygen as can be observed in Figure 2. Chemical generation of higher oxidation states derived from **2** were carried out at pH 1.0 in a 0.1 M triflic acid solution using Ce^{IV} as an oxidant. In this manner oxidation states II,II, II,III, III,III, and IV,III could be characterized by UV/Vis spectroscopy (see the Supporting Information). In agreement with the electrochemical results, the addition of one more equivalent of Ce^{IV} generates dioxygen quickly and thus precludes the easy spectroscopic characterization of oxidation state IV,IV.

Addition of excess of Ce^{IV} in a 0.1 M triflic acid solution generates bubbles as a result of the formation of dioxygen. In particular, the system having 1.5 mM **2**/100 mM Ce^{IV}/pH 1.0 in 0.1 M triflic acid generates 30 μmols of dioxygen, thus representing a respectable turnover number (TON) of 9.6 with an initial turnover frequency (TOF_i [moles of oxygen/moles of catalyst)/time]) of $31 \times 10^{-3}\ s^{-1}$. The oxygen generated was measured both by manometry and by a Clark electrode in the gas phase with exquisite agreement between both techniques, as can be seen in Figure 3.

It is very interesting to note here that **4** under similar reaction conditions gives a $TOF_i = 3.3 \times 10^{-3}\ s^{-1}$, which is nine times lower than that for **2**. It thus constitutes an example of how the electronic consequences of replacing the bpea ligand by tpym significantly impact the initial rates of oxygen generation. Furthermore, **6** has a TOF_i of $49 \times 10^{-3}\ s^{-1}$ which is about 60% larger than that of **2** and an order of magnitude

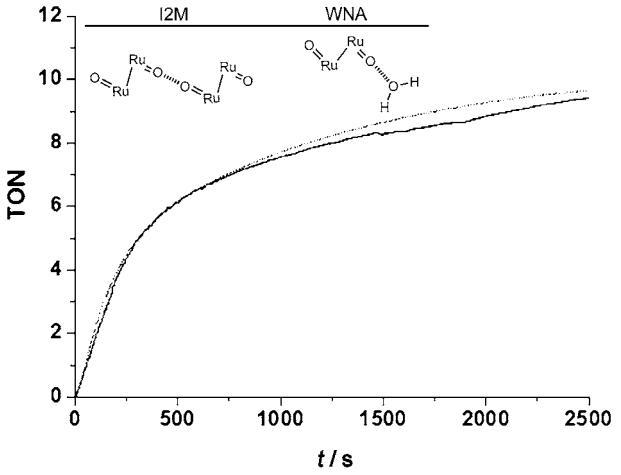

Figure 3. Oxygen evolution profiles monitored simultaneously by manometry (dotted line) and gas phase Clark electrode (solid line). Profiles obtained by adding 100 mM Ce^{IV} to 1.5 mM **2**. Inset: sketch of possible reaction mechanisms depending on the O–O bond-formation route.

higher than that of **4**. For **6** a thorough mechanistic study shows that the critical O–O bond-formation step involves an intramolecular O···O interaction.[4c]

For complexes **2** and **4** this is not possible because of the geometric constraint imposed by the facial geometry of the tridentate ligand. Therefore for complexes **2** and **4** two potential mechanisms are possible: 1) the interaction of two M-O units (I2M) in a bimolecular fashion or 2) a water nucleophilic attack of a solvent water molecule onto an M-O unit (WNA) (inset of Figure 3).

To investigate the nature of the mechanism both kinetic analysis based on initial velocities (v_i) of oxygen formation under catalytic conditions, and ^{18}O-labeling studies were carried out. Figure 4, shows a plot of oxygen generation versus time for concentrations of **2** ranging from 0.5–1.3 mM

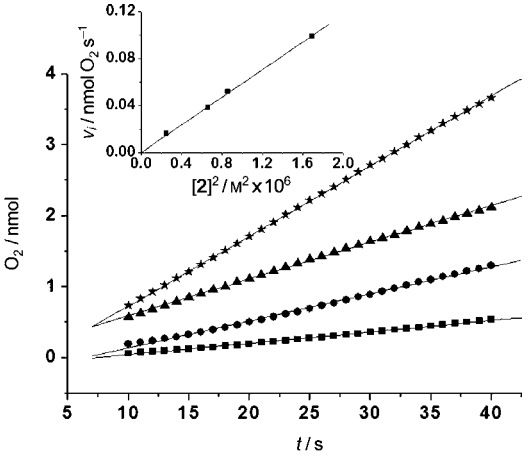

Figure 4. Plot of oxygen evolution vs. time obtained at the initial stages of the reaction by adding 100 mM Ce^{IV} oxidant to a catalyst solution containing 0.50 (squares), 0.81 (circles), 0.93 (triangles), and 1.30 mM (stars) **2**. Inset: plot of oxygen generation initial velocities (v_i) vs. $[\mathbf{2}]^2$. All experiments were carried out in 0.1 M aqueous triflic acid solution at 298 K with a total volume of 2 mL.

while maintaining the Ce^{IV} concentration constant at 100 mM. The v_i collected in this manner were then plotted versus the quadratic catalyst concentration as shown in the inset of Figure 4, thereby giving a linear fit that bisects the *y* axis at zero. In contrast the v_i were found to have a complex behavior with regard to $[Ce^{IV}]$.

The second-order behavior with regard to [Ru] point towards a rate-determining step involving a bimolecular O–O bond-formation step. Thus based on kinetic analysis a bimolecular I2M mechanism, as shown in Scheme 1, is proposed to

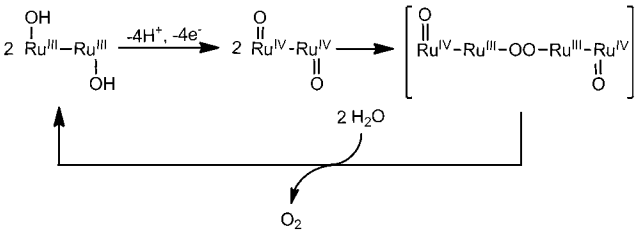

Scheme 1. Proposed reaction mechanism.

occur for complex **2**. To further support the kinetic analysis ^{18}O-labeling experiments were carried out and the results are reported in Table 3. The experiments were performed by adding 5 equivalents of Ce^{IV}, dissolved in a 0.1M triflic acid

Table 3: Relative isotopic ratios of O_2 evolved from the first metal cycle at different degrees of solvent labeling, along with the calculated values assuming different reaction mechanisms.

Entry	^{18}O[a]		Isotopic ratios			
	Solv.	O_2	Exch.[b]	WNA[c]	I2M[d]	Expl.
1	19.4	$^{16}O_2$	65.0	80.4	99.5	99.1
2		$^{16}O^{18}O$	31.3	19.5	0.5	0.9
3		$^{18}O_2$	3.8	0.05	6×10^{-4}	0.0
4	12.0	$^{16}O_2$	77.4	88.0	99.5	99.3
5		$^{16}O^{18}O$	21.1	12.0	0.5	0.7
6		$^{18}O_2$	1.4	2×10^{-4}	4×10^{-4}	0.0

[a] Degree of solvent ^{18}O labeling [%]. [b] Exch.: expected ratios in case of a fast O atom exchange between the catalyst and the solvent. [c] WNA: expected ratios for the mechanism involving a nucleophilic attack of a solvent water to the O atom of a Ru–O group. [d] I2M: expected ratios for the mechanism involving a bimolecular mechanism with an oxygen–oxygen coupling from two Ru–O groups of different catalyst molecules.

solution in 99.8% $H_2{}^{18}O$, to a solution of **2** in H_2O, and the oxygen generated was analyzed on-line by mass spectrometry. The experiments were done at two different degrees of labeling and in both cases they give an unambiguous agreement for an O–O bond formation taking place by the interaction of two Ru-O units in a bimolecular fashion.

In summary, a new dinuclear Ru^{II} complex **2**, having the Ru-OH_2 groups in a *trans* disposition, is reported to be capable of catalytically oxidizing water into dioxygen. The complex is stable up to the oxidation state III,IV. Additional oxidation to the IV,IV state generates oxygen. The *trans* disposition of the Ru-OH_2 imposed by the facial tpym ligands

precludes the possibility of an intramolecular I2M mechanism for the critical O–O bond-formation step. This data is in sharp contrast with the related and thoroughly studied Ru-Hbpp complex **6**, wherein the two Ru-OH_2 groups are arranged in a *cis* manner and whose mechanism is an intramolecular I2M. For **2**, two options are possible for the O–O bond-formation step: either a water nucleophilic attack or a bimolecular I2M mechanism (see inset Figure 3). The quadratic dependence of the initial O_2 formation velocities on [**2**] (see inset Figure 4) together with the labeling experiments provide compelling evidence that the formation of dioxygen in this complex occurs through a bimolecular I2M mechanism. The combination of all this mechanistic evidence is summarized in Scheme 1. The present report constitutes the first example where a successful ^{18}O-labeling experiment demonstrates, unambiguously, the presence of this bimolecular step as the only mechanistic route.

Received: February 17, 2012
Revised: March 22, 2012
Published online: April 30, 2012

Keywords: oxidation · redox catalysis · ruthenium · transition metals · water chemistry

[1] a) N. S. Lewis, D. G. Nocera, *Proc. Natl. Acad. Sci. USA* **2006**, *43*, 15729; b) A. Llobet, F. Meyer, *Angew. Chem.* **2011**, *123*, A30; *Angew. Chem. Int. Ed.* **2011**, *50*, A30 (DFG special insert); c) S. Y. Reece, J. A. Hamel, K. Sung, T. D. Jarvi, A. J. Esswein, J. J. H. Pijpers, D. G. Nocera, *Science* **2011**, *334*, 645.

[2] a) Y. Umena, K. Kawakami, J.-R. Shen, N. Kamiya, *Nature* **2011**, *473*, 55–60; b) M. Haumann, P. Liebisch, C. Müller, M. Barra, M. Grabolle, H. Dau, *Science* **2005**, *310*, 1019.

[3] New Science for a Secure and Sustainable Energy Future. Basic Energy Science Advisory Committee, **2008** (US Department of Energy, Washington DC).

[4] a) S. W. Gestern, G. J. Samuels, T. J. Meyer, *J. Am. Chem. Soc.* **1982**, *104*, 4029–4030; b) R. Zong, P. Thummel, *J. Am. Chem. Soc.* **2005**, *127*, 12802; c) S. Romain, F. Bozoglian, X. Sala, A. Llobet, *J. Am. Chem. Soc.* **2009**, *131*, 2768–2769; d) Y. Xu, A. Fischer, L. Duan, L. Tong, E. Gabrielsson, B. Åkermark, L. Sun, *Angew. Chem.* **2010**, *122*, 9118–9121; *Angew. Chem. Int. Ed.* **2010**, *49*, 8934–8937.

[5] a) H. W. Tseng, R. Zong, J. T. Muckerman, R. Thummel, *Inorg. Chem.* **2008**, *47*, 11763–11773; b) J. J. Concepcion, J. W. Jurss, J. L. Templeton, T. J. Meyer, *J. Am. Chem. Soc.* **2008**, *130*, 16462–16463; c) S. Roeser, P. Farras, F. Bozoglian, M. Martínez-Belmonte, J. Benet-Buchholz, A. Llobet, *ChemSusChem* **2011**, *4*, 197–207.

[6] a) W. C. Ellis, N. D. McDaniel, S. Bernhard, T. J. Collins, *J. Am. Chem. Soc.* **2010**, *132*, 10990–10991; b) D. W. Wasylenko, C. Ganesamoorthy, C. P. Berlinguette, *Chem. Commun.* **2011**, *47*, 4249–4251.

[7] a) N. D. McDaniel, F. J. Coughlin, L. L. Tinker, S. Bernhard, *J. Am. Chem. Soc.* **2008**, *130*, 210–217; b) J. D. Blakemore, N. D. Schley, D. Balcells, J. F. Hull, G. W. Olack, C. D. Incarvito, O. Eisenstein, G. W. Brudvig, R. H. Crabtree, *J. Am. Chem. Soc.* **2010**, *132*, 16017.

[8] a) Z. Chen, J. J. Concepcion, H. Luo, J. F. Hull, A. Paul, T. J. Meyer, *J. Am. Chem. Soc.* **2010**, *132*, 17670–17673; b) D. J. Wasylenko, C. Ganesamoorthy, M. A. Henderson, B. D. Koivisto, H. D. Osthoff, C. P. Berlinguette, *J. Am. Chem. Soc.* **2010**, *132*, 16094–16106; c) F. Bozoglian, S. Romain, M. Z. Ertem, T. K. Todorova, C. Sens, J. Mola, M. Rodríguez, I. Romero, J. Benet-Buchholz, X. Fontrodona, C. J. Cramer, L. Gagliardi, A. Llobet, *J. Am. Chem. Soc.* **2009**, *131*, 15176–15187.

[9] a) F. Laurent, E. Plantalech, B. Donnadieu, A. Jimenez, F. Hernandez, M. Martinez-Ripoll, M. Biner, A. Llobet, *Polyhedron* **1999**, *18*, 3321–3331; b) I. Romero, M. Rodriguez, A. Llobet, M. N. Collomb-Dunand-Sauthier, A. Deronzier, T. Parella, H. Soteckli-Evans, *J. Chem. Soc. Dalton Trans.* **2000**, 1689–1694; c) X. Sala, E. Plantalech, A. Poater, M. Rodriguez, I. Romero, M. Sola, A. Llobet, S. Jansat, M. Gomez, H. Stoeckli-Evans, J. Benet-Buchholz, *Chem. Eur. J.* **2006**, *12*, 2798–2807; d) C. Sens, M. Rodríguez, I. Romero, A. Llobet, T. Parella, J. Benet-Buchholz, *Inorg. Chem.* **2003**, *42*, 8385–8394; e) E. Masllorens, M. Rodríguez, I. Romero, A. Roglans, T. Parella, J. Benet-Buchholz, M. Poyatos, A. Llobet, *J. Am. Chem. Soc.* **2006**, *128*, 5306–5307; f) N. Planas, G. J. Christian, S. Roeser, E. Mas-Marzá, M. R. Kollipara, J. Benet-Buchholz, F. Maseras, A. Llobet, *Inorg. Chem.* **2012**, *51*, 1889–1901.

[10] J. Mola, C. Dinoi, X. Sala, M. Rodríguez, I. Romero, T. Parella, X. Fontrodona, A. Llobet, *Dalton Trans.* **2011**, *40*, 3640–3646.

[11] C. Sens, I. Romero, M. Rodríguez, A. Llobet, T. Parella, J. Benet-Buchholz, *J. Am. Chem. Soc.* **2004**, *126*, 7798–7799.

[12] S. Roeser, M. Z. Ertem, C. Cady, R. Lomoth, J. Benet-Buchholz, L. Hammarström, B. Sarkar, W. Kaim, C. J. Cramer, A. Llobet, *Inorg. Chem.* **2012**, *51*, 320–327.

